IEEE Transactions on Automation Science and Engineering (T-ASE) paper, presented at ICRA 2024, Yokohama, Japan. Cite as T-ASE paper.

Contact Force Estimation of Robot Manipulators With Imperfect Dynamic Model: On Gaussian Process Adaptive Disturbance Kalman Filter

Yanran Wei , Shangke Lyu , Wenshuo Li* , Xiang Yu , *Senior Member, IEEE,* and Lei Guo , *Fellow, IEEE*

***Abstract*—This paper is concerned with the contact force estimation problem of robot manipulators based on imperfect dynamic models of the manipulator and the contact force. To handle the imperfect dynamic information of the manipulator, a hybrid model, consisting of the nominal model and the residual dynamics, is established for the manipulator, and the Gaussian process regression (GPR) technique is employed to learn the mean and covariance of the residual dynamics. On this basis, a virtual measurement equation is established for contact force estimation and a Gaussian process adaptive disturbance Kalman filter (GPADKF) is developed where the variational Bayes technique is employed to achieve online identification of the noise statistics in the force dynamics. The GPADKF is capable of decoupling the contact force from residual dynamics and system noises, thereby reducing the dependence on accurate dynamic models of the manipulator and the contact force. Simulation and experimental results demonstrate that the proposed scheme outperforms the state-of-art methods.**

***Note to Practitioners*—Contact force estimation for robot manipulators can be achieved by fusing the dynamic models of the manipulator and the contact force. When both models are imprecise, the traditional inverse dynamics-based and disturbance Kalman filter-based approaches can no longer provide accurate force estimates. To handle this challenge, a computationally efficient hybrid dynamic model is established for the manipulator, which consists of the nominal model and a residual dynamics compensation term learned from offline data via the GPR. On this basis, an adaptive disturbance Kalman filter is constructed by using the variational Bayes technique to deal with the inaccurate noise covariance matrix in the force dynamic model. Compared with the existing approaches, the force estimate obtained via the proposed scheme is more accurate and reliable, as refined noise covariance matrices (provided by both the GPR and the variational Bayes procedure) have been adopted in the Kalman gain calculation. The proposed GPADKF method is the extension of the composite disturbance filtering (CDF) framework. With the proposed scheme, the dependency on the perfect dynamic models in contact force estimation can be significantly reduced, and this makes our approach especially suitable for contact force estimation problems under unfamiliar and complicated environments.**

***Index Terms*—Force estimation, Disturbance observer, Gaussian process, Disturbance Kalman filter, Robot manipulator.**

I. Introduction

THE problem of contact force estimation of robot manipulators has attracted extensive research attention due to the progressive demand for manipulation performance and safety of the robot. As a central issue in robotic operation tasks, contact forces are prevalent across various types of robotic systems, including but not limited to industrial robots, surgical robots, and space manipulators [1]. Force estimation techniques can be used for interactive environment perception and robot compliance control tasks such as cooperative handling and precise assembly [2]. Due to the extra cost and workload of the force sensors [3], sensorless methods requiring no additional sensors have gained increasing popularity in recent years.

The main idea of sensorless force estimation is to construct a force observer based on the dynamic model of the robot manipulator. In this case, the performance of force estimation depends heavily on the model accuracy. Typically, the Euler-Lagrange method can be used to establish a standard physics-based dynamic model [4] and linear regression is adopted for parameter identification [5], [6]. However, the dynamic model thus established would become increasingly inaccurate due to parameter drift, mechanical structure damage, and actuator degradation [7]. This is particularly true for non-industrial robots. In fact, non-industrial robots are usually low in stiffness and with limited actuation power, which implies that the impact of residual dynamics is more significant for non-industrial robots as compared to industrial robots. In addition, the components of non-industrial robots can exhibit large variations concerning their specifications, especially in complex and changing environments such as severe weather conditions [8]. Therefore, decoupling residual dynamics from the contact force signal is an important demand, especially under highly uncertain interactive environments.

This research was supported by the National Natural Science Foundation of China (Grant numbers 62003018, 61903019, 61973012, 62003016 and 61833013), the Program for Changjiang Scholars and Innovative Research Team (Grant number IRT 16R03), National Key Research and Development Program of China (Grant number 2020YFA0711200), Defense Industrial Technology Development Program (Grant number JCKY2020601C016), Key Research and Development Program of Zhejiang (Grant number 2021C03158), Natural Science Foundation of Zhejiang Province (Grant Numbers LD21F030001 and LQ20F030006), Science and Technology Key Innovative Grant of Hangzhou (Grant number 20182014B06).

Y. Wei, X. Yu and L. Guo are with the School of Automation Science and Electrical Engineering, Beihang University, Beijing 100191, China. E-mail: yrweibuaa@126.com, {xiangyu_buaa, lguo}@buaa.edu.cn.

L. Lyu is with Machine Intelligence Lab (MiLAB), School of Engineering, Westlake University, Hangzhou 310024, China. E-mail: lyushangke@westlake.edu.cn.

W. Li is with Hangzhou Innovation Institute, Beihang University, Hangzhou 310051, China. E-mail: wslibuaa@126.com.

(Corresponding author: Wenshuo Li.)

IEEE Transactions on Automation Science and Engineering (T-ASE) paper, presented at ICRA 2024, Yokohama, Japan.

Although various degrees of success have been achieved by the existing approaches, there are still several technical challenges identified as follows.

1) *Refined quantification of multi-source uncertainties.* On one hand, the errors that occur during the offline model learning phase may propagate into the online force estimation. On the other hand, the noise covariance matrices in the dynamic equation of the contact force are usually inaccurate, especially in unstructured environments where priori information is incomplete. Therefore, it is necessary to address these challenges by effectively characterizing the underlying multi-source uncertainties and establishing an enhanced dynamic model for contact force estimation.
2) *Contact force estimation under multi-source uncertainties.* The force estimation model is subject to residual dynamics (modeling errors of the robot manipulator), errors in residual dynamics learning, as well as inaccurate modeling of the contact force dynamics. The heterogeneous characteristic of these uncertainties has a substantial impact on force estimation, posing a formidable challenge in designing observers for contact force estimation amidst multi-source uncertainties [9].

Stimulated by the aforementioned challenges, a novel force estimation scheme termed *Gaussian process adaptive disturbance Kalman filter* (GPADKF) is developed in this article. We aim to simultaneously take into consideration the residual dynamics, errors in residual dynamics learning, and inaccuracies in the contact force model, each of which can potentially lead to filter divergence. Specifically, a semi-parametric dynamic model named the enhanced Gaussian process (EGP) model with residual dynamics learning via Gaussian process regression (GPR) was established. On this basis, we propose an adaptive disturbance Kalman filter (DKF) that leverages the learned mean value of residual dynamics through GPR to construct a compensation term in the measurement equation. Additionally, the covariance matrices obtained from GPR are incorporated in the tuning of the filter gain, while inaccurate covariance matrices in the force dynamics are addressed using variational Bayesian (VB) approximation [10]. The overall architecture of the proposed scheme is illustrated in Fig.1. It should be noted that the proposed GPADKF method can be viewed as a realization of the generic composite disturbance filtering (CDF) framework, where the main idea is to separate the dynamic and stochastic uncertainties by explicitly utilizing their characteristics [9], [11].

The main contributions of our work are two-fold:

1) By using GPR to approximate the residual dynamics, a hybrid EGP model is established. The EGP model enables residual dynamics compensation (via the mean value of residual dynamics) and refined quantification of uncertainties (characterized by the covariance matrices). Compared with the existing models [8], [12], [13], the EGP model can lay a solid foundation for the *cautious* force estimation as the stochastic uncertainties are comprehensively characterized by confidence;
2) On the basis of the EGP model, the GPADKF scheme proposed in our work can offer an accurate force estimate in the presence of multi-source uncertainties. Specifically, the residual dynamics are compensated for and the stochastic noises are attenuated based on precise statistics quantification (via both GPR and VB). When compared to traditional DKF methods (without residual dynamics compensation), the proposed scheme is capable of decoupling the residual dynamics from the force estimate. Compared with the enhanced DKF (EDKF) [12] that uses the mean value (learned by neural networks) for compensation, the GPADKF can provide a more cautious force estimate as more accurate noise covariance matrices have been adopted in the Kalman gain calculation.

The rest of this paper is organized as follows. In Section II, related works are summarized in detail. In Section III, problem statement and preliminaries are presented. In Section IV, residual dynamic model learning and the EGP system modeling are described. In Section V, the GPADKF algorithm is elaborated and simulation results are given. In Section VI, experimental results are presented to demonstrate the effectiveness of the EGP model and the superiority of the GPADKF. Concluding remarks are provided in Section VII.

II. Related Works

Two primary technical approaches have been employed to enhance the accuracy of force estimation: 1) improving the accuracy of the robot manipulator model, and 2) employing advanced force estimation techniques.

To improve the model accuracy of robot manipulators, the data-driven methods have been introduced to learn the dynamic model from historical data by using neural networks (NNs) [12], [14] and statistical non-parametric methods [8], [13], [15], [16]. These learning-based techniques have a strong capability in approximating the inherent nonlinearities in the data. However, purely data-driven methods lack interpretability and suffer from high computational burden [7]. To cope with these challenges, a semi-parametric model has been presented in [12] to obtain an accurate dynamic model of the robot manipulator without excessive computational burden. The semi-parametric model is in essence a hybrid model which incorporates the residual dynamics learned by the NN into the nominal model. However, due to the lack of characterization of uncertainties arising from the learning process, it becomes challenging to assess the confidence of the learned model in the force observer design therein.

Fortunately, the GPR provides an efficient non-parametric probabilistic framework for model learning, which is naturally compatible with the Bayesian filtering procedure [17]–[19]. In addition to predicting the mean value of residual dynamics, GPR can also quantify the uncertainties in the learned models, which are represented by the covariance matrices [20]. Therefore, the model learned via GPR has excellent potential for more *accurate* and *reliable* force estimation when combined with the Bayesian filter.

From the aspect of force estimation, the main representative approaches include generalized momentum observer

IEEE Transactions on Automation Science and Engineering (T-ASE) paper, presented at ICRA 2024, Yokohama, Japan.

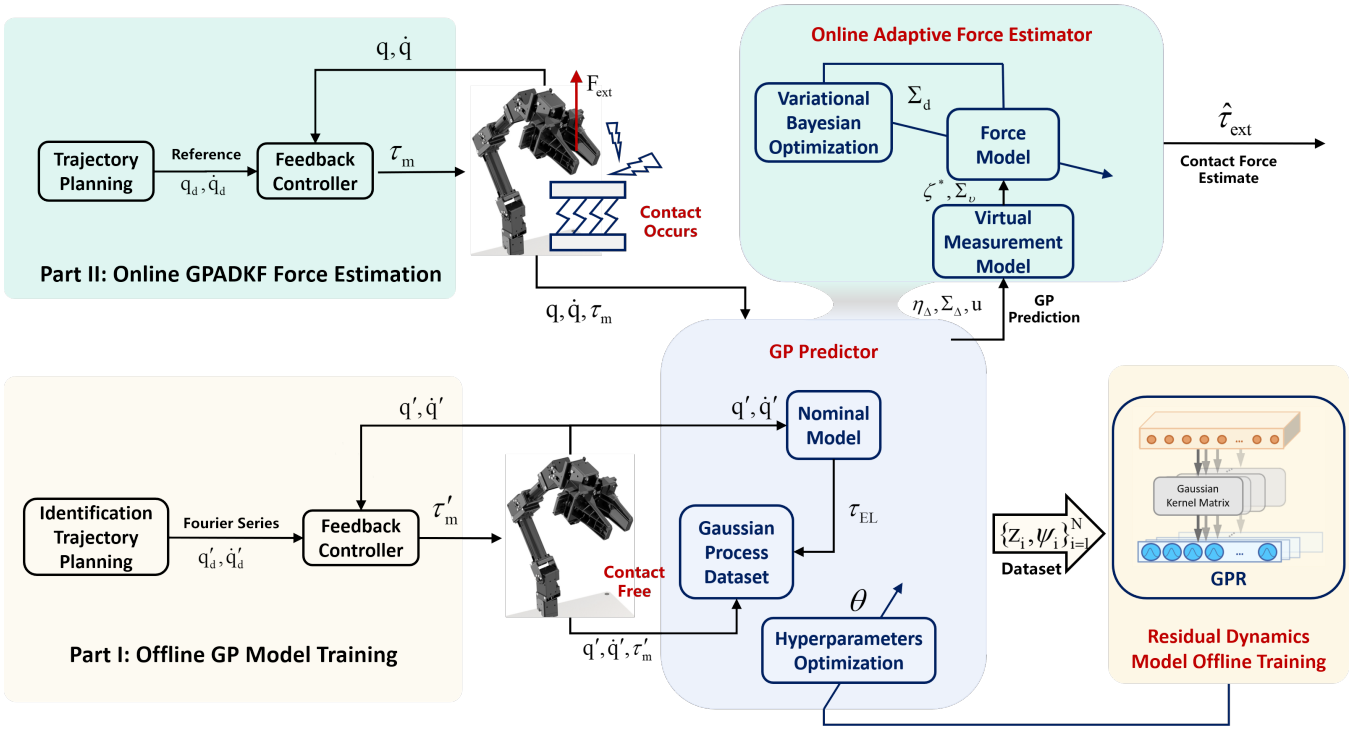

Figure 1. Illustration of the proposed force estimation architecture. The shaded zones with different colors indicate different phases of the proposed scheme. The complete architecture comprises two parts. Part I, delineated with a beige-shaded region, depicts the offline training phase for the residual dynamics. Part II, demarcated by a light green shaded area, illustrates the online force estimation stage. Note that the light blue shaded area is the GP predictor which appears in both the offline learning and the online prediction phases. Furthermore, the blocks with dark blue text form the proposed GPADKF algorithm.

(GMO) [21]–[23], frequency-domain disturbance observer (DO) [24], [25], time-domain nonlinear DO (NDO) [26]–[31], [32], impedance control based 6-D virtual sensor [33]–[35], filter-based methods [12], [36], [37], to name just a few. In [21], the GMO-based force observer has been employed in manipulator collision detection without requiring acceleration measurement. In [25], the frequency-domain DO has been adopted as the contact force observer to perceive the interactive environmental impedance of manipulators. In [26], a series of NDOs for unknown disturbance estimation of nonlinear and coupled systems have been summarized. An early result on applying NDO to estimate the contact forces of the robot manipulator can be found in [30]. [32] has established a refined DO, a powerful tool for effectively separating and estimating multiple disturbances, such as torque signals with priori knowledge and norm-bounded torque signals. In [33], reliable force estimation has been achieved via a virtual sensor within a unified framework where the sensorless Cartesian impedance controller and the extended Kalman filter (EKF) are employed for interactive control and interaction wrench estimation, respectively. In [12], the DKF has been used as the force observer with an enhanced robustness against residual dynamics, which essentially belongs to a type of EDKF method. In our recent work [36], an EDKF approach has been proposed, which aims to address residual dynamics and errors in residual dynamics learning. Nevertheless, similar to the aforementioned methods, the result in [36] is based on the assumption that an accurate dynamic model of the contact force (including precise knowledge of the noise statistics) is available prior to the force estimation task. For better clarity, the pros and cons of some typical force estimation methods, including the proposed one, are summarized in Table I.

III. Problem Statement and Preliminaries

In this section, we formulate the force estimation problem and briefly introduce the GPR method that will be used in residual dynamics learning.

A. Problem Statement

We consider robot manipulators as open kinematic chains of rigid bodies, consisting of n rigid joints and contact with the environment directly. The generalized coordinates $\mathbf{q} \in \mathbb{R}^n$ can be associated with the position of the links. The standard physical dynamic model is

$$\mathbf{M}(\mathbf{q})\ddot{\mathbf{q}} + \mathbf{C}(\mathbf{q}, \dot{\mathbf{q}})\dot{\mathbf{q}} + \mathbf{G}(\mathbf{q}) = \boldsymbol{\tau}_m - \boldsymbol{\tau}_{ext} - \boldsymbol{\tau}_\Delta, \quad (1)$$

where $\mathbf{q}, \dot{\mathbf{q}}, \ddot{\mathbf{q}} \in \mathbb{R}^n$ denote the joint position, velocity, and acceleration, respectively; $\mathbf{M}(\mathbf{q}) \in \mathbb{R}^{n\times n}$ is the symmetric positive-definite inertia matrix; $\mathbf{C}(\mathbf{q}, \dot{\mathbf{q}})\dot{\mathbf{q}} \in \mathbb{R}^n$ is the Coriolis and centripetal vector; $\mathbf{G}(\mathbf{q}) \in \mathbb{R}^n$ is the gravity vector; $\boldsymbol{\tau}_m \in \mathbb{R}^n$ and $\boldsymbol{\tau}_\Delta \in \mathbb{R}^n$ denote the active motor torque and the unmodeled residual dynamics, respectively; $\boldsymbol{\tau}_{ext} \in \mathbb{R}^n$ represents the equivalent external torque. The nominal model is established based on the following Euler-Lagrange equation

$$\boldsymbol{\tau}_{EL} = \mathbf{M}(\mathbf{q})\ddot{\mathbf{q}} + \mathbf{C}(\mathbf{q}, \dot{\mathbf{q}})\dot{\mathbf{q}} + \mathbf{G}(\mathbf{q}), \quad (2)$$

IEEE Transactions on Automation Science and Engineering (T-ASE) paper, presented at ICRA 2024, Yokohama, Japan.

Table I
COMPARISON OF DIFFERENT FORCE ESTIMATION METHODS

Method	Residual dynamics compensation	Refined uncertainties quantification	Contact force model correction	Measurement noise attenuation
GMO [21]–[23]	×	×	×	Sub-optimal
DO [24], [25]	×	×	×	Sub-optimal
NDO [26]–[32]	×	×	×	Sub-optimal
DKF [37]	×	×	×	Optimal
EDKF [12], [36]	✓	×	×	Optimal
GPADKF	✓	✓	✓	Optimal

where $\boldsymbol{\tau}_{EL}$ represents the torque computed using the nominal model [38].

Property 1: The matrix $\dot{\mathbf{M}}(\mathbf{q}) - 2\mathbf{C}(\mathbf{q}, \dot{\mathbf{q}})$ is skew-symmetric, which is equivalent to

$$\dot{\mathbf{M}}(\mathbf{q}) = \mathbf{C}(\mathbf{q}, \dot{\mathbf{q}}) + \mathbf{C}^T(\mathbf{q}, \dot{\mathbf{q}}). \tag{3}$$

The relationship between the external torque and the contact force can be obtained as

$$\boldsymbol{\tau}_{ext} = \mathbf{J}(\mathbf{q})^T \mathbf{F}_{ext}, \tag{4}$$

where $\mathbf{J}(\mathbf{q}) \in \mathbb{R}^{6\times n}$ is the Jacobian matrix and $\mathbf{F}_{ext} = [\mathbf{f}_{ext}^T, \mathbf{m}_{ext}^T]^T \in \mathbb{R}^6$ is the contact force exerted on the end effector of the manipulator.

Ideally, the manipulator dynamics are completely characterized by an appropriate physical model, i.e., $\boldsymbol{\tau}_\Delta = 0$. Assuming no residual dynamics, the contact force estimation can be obtained from (1) as

$$\hat{\mathbf{F}}_{ext} = \mathbf{J}(\mathbf{q})(\mathbf{M}(\mathbf{q})\ddot{\mathbf{q}} + \mathbf{C}(\mathbf{q}, \dot{\mathbf{q}})\dot{\mathbf{q}} + \mathbf{G}(\mathbf{q}) - \boldsymbol{\tau}_m). \tag{5}$$

In practical scenarios, however, residual dynamics invariably exist, resulting in a deviation in force estimation $\hat{\mathbf{F}}_{ext} = \mathbf{F}_{ext} - \mathbf{J}(\mathbf{q})\boldsymbol{\tau}_\Delta$. Therefore, it is imperative to consider the impact of residual dynamics $\boldsymbol{\tau}_\Delta$, which impairs the accuracy of force estimation, during the design of the force observer.

Due to the challenge of separating contact force from residual dynamics, the estimation of pure contact force using sensorless methods becomes considerably arduous. To tackle this issue, various effective techniques have been employed, such as time-variant thresholds [39], identification of parametric uncertainties [40], and feedback-control-based approaches [41] for compensating or suppressing residual dynamics. However, these methods have only utilized limited information regarding the residual dynamics, such as norm-bounded or partially known structures, which is inadequate for achieving accurate force estimation. It is evident that additional information on the residual dynamics needs to be leveraged. In this paper, we propose the adoption of GPR to learn a predictive model of the residual dynamics, which will be subsequently utilized for online compensation.

Remark 1. *The residual dynamics results from various physical factors such as friction torques, inertial matrix uncertainty and measurement errors. The mathematical model of residual dynamics is quite complicated (state-dependent) and cannot be simply described as a slowly time-varying or norm-bounded signal. Therefore, learning-based techniques such as NN and GPR are better employed to provide a more accurate model for the residual dynamics.*

B. Gaussian Process Regression

GPR is a powerful, non-parametric tool for learning and describing the underlying regression functions through observed data in the form of distributions over functions.

For GPR, measurement outputs are drawn from a noisy process, that is,

$$\mathbf{y} = g(\mathbf{z}) + \epsilon, \tag{6}$$

with $\epsilon \sim \mathcal{N}(0, \sigma_n^2)$ being zero-mean Gaussian white noise with variance σ_n^2. Here, the data set $\mathcal{D} = \{\mathbf{z}_i, \mathbf{y}_i\}_{i=1}^N$ contains previously collected N data points with inputs $\mathbf{Z} = [\mathbf{z}_1, \ldots, \mathbf{z}_N]^T \in \mathbb{R}^{N\times D_z}$ and outputs $\mathbf{Y} = [\mathbf{y}_1, \ldots, \mathbf{y}_N]^T \in \mathbb{R}^{N\times D_y}$.

The GPR modeling is based on the assumption that a random vector consisting of any N variables obeys a multivariate joint Gaussian distribution. In other words, the process to be learned is assumed to be a Gaussian process (GP), i.e., $g(\mathbf{z}) \sim \mathcal{GP}(m(\mathbf{z}), k(\mathbf{z}, \mathbf{z}))$. Note that each output dimension is trained individually, which means that the components of $\mathbf{y}_i$ are independent. A GP is completely defined in each output dimension $a \in \{1, \ldots, D_y\}$ by a scalar mean function $m^a(\cdot)$ and a positive semi-definite kernel function $k^a(\cdot, \cdot)$, specifying the covariance between pairs of inputs.

The GPR method typically involves selecting appropriate priori distributions and stylizing hyperparameter optimization. Typically, the most popular option is the zero mean function paired with the squared exponential (SE) kernel function with additive noise, that is,

$$k(\mathbf{z}_i, \mathbf{z}_j) = \sigma_f^2 \exp(-\frac{1}{2}(\mathbf{z}_i - \mathbf{z}_j)^T \boldsymbol{\Lambda}^{-1}(\mathbf{z}_i - \mathbf{z}_j)) + \sigma_n^2 \delta_{ij}, \quad i, j = 1, \ldots, N, \tag{7}$$

where σ_f^2 is the variance, δ_{ij} is the Kronecker delta function, $\boldsymbol{\Lambda} = \mathrm{diag}(l_1, l_2, \ldots, l_{D_z})$ is a positive diagonal length-scale matrix, and σ_n^2 is the variance of the global noise ϵ in (6). The length scales reflect the relative smoothness along each input dimension. The SE kernel in (7) is commonly utilized as the covariance function due to its compatibility with sparse approximation methods.

The hyperparameters of a GP, including the parameters of the mean and covariance functions, as well as

IEEE Transactions on Automation Science and Engineering (T-ASE) paper, presented at ICRA 2024, Yokohama, Japan.

the global noise variance, are denoted as a vector $\boldsymbol{\theta} = [\sigma_{f,1}^2, \ldots, \sigma_{f,N}^2, \sigma_n^2, l_1, \ldots, l_{ND_z}]$. The training process of a GP involves obtaining the maximum a posteriori (MAP) estimate of these hyperparameters. Within the Bayesian inference framework, the distribution of the hyperparameters is proportional to the marginal likelihood, given by

$$p(\boldsymbol{\theta}|\mathbf{Z}, \mathbf{Y}) \propto \frac{1}{(2\pi)^{\frac{N}{2}}\sqrt{\det(\mathbf{K})}}\exp(-\frac{1}{2}\mathbf{Y}^{\mathrm{T}}\mathbf{K}^{-1}\mathbf{Y}). \quad (8)$$

At each test point $\mathbf{z}_*$, the predictive distribution of the outputs in each dimension a is Gaussian with mean $\mu^a(\cdot)$ and covariance matrix $\Sigma^a(\cdot)$, which are given by

$$\mu^a(\mathbf{z}_*) = m^a(\mathbf{z}_*) + \mathbf{k}_{\mathbf{z}_*\mathbf{Z}}^T K^{-1}(\mathbf{y} - \mathbf{m}^a(\mathbf{Z})), \quad (9a)$$

$$\Sigma^a(\mathbf{z}_*) = k_{\mathbf{z}_*\mathbf{z}_*} - \mathbf{k}_{\mathbf{z}_*\mathbf{Z}}^T K^{-1}\mathbf{k}_{\mathbf{z}_*\mathbf{Z}}, \quad (9b)$$

where we use the shorthand $k_{ab} := k(a, b)$ for brevity. The dimensions of the mean function and covariance function are matched, indicated by the equalities where $m(\mathbf{z}) : \mathbb{R}^{D_z} \to \mathbb{R}^{D_z}$ and $k_{\mathbf{z}1,\mathbf{z}2} : \mathbb{R}^{D_{z1}} \times \mathbb{R}^{D_{z2}} \to \mathbb{R}^{D_{z1}\times D_{z2}}$. $\mathbf{z}_*$ and $\mathbf{Z}$ represent prediction points and training points, respectively. $K = k_{\mathbf{Z},\mathbf{Z}} + \sigma_n^2 I$ is the Gram matrix with additive noise.

Remark 2. *The prediction of the GP enables the reflection of correlations between inputs. Apart from providing the mean value of the residual dynamics, GP also offers the capability to quantify prediction uncertainties through its covariance function, which grants it a distinct advantage over other learning-based methods. Moreover, due to its non-parametric structure, GP serves as a more potent approach for nonlinear model learning. Furthermore, as a sample-efficient method, GP can achieve modeling learning with a smaller sample size, which matches the requirement of our work. Due to the aforementioned merits, the GP can be used as an effective online predictor and compensator for more cautious estimation and control. However, the time required for online prediction of GP increases sharply with the size of the training dataset, which is the main disadvantage of the GPR method. To avoid excessive time costs, the data acquisition process needs to be optimized to ensure a small-sized and informative training dataset.*

IV. Enhanced Gaussian Process Model

In this section, a hybrid EGP model will be developed by integrating GPR prediction into the dynamic equation of the manipulator. More specifically, the residual dynamics learned through GPR will be presented in Section IV-A, while the comprehensive EGP model including a generalized momentum model and multi-source disturbances will be discussed in Section IV-B.

A. Residual Dynamics Model Learning with GPR

In practice scenarios, the residual dynamics existing in the dynamic model of an n-DOF manipulator can stem from various factors, including but not limited to [21]:

- Position and velocity measurement errors, denoted as $\Delta q(n_q)$ and $\Delta\dot{q}(n_{\dot{q}})$ respectively, can arise from measurement noises n_q and $n_{\dot{q}}$;
- Friction torque, represented as $\boldsymbol{\tau}_F \in \mathbb{R}^n$, can be modeled as [6]
$$\boldsymbol{\tau}_F = \mathbf{Fc} \cdot \mathrm{sign}(\dot{\mathbf{q}}) + \mathbf{Fv} \cdot \dot{\mathbf{q}} + \mathbf{B}, \quad (10)$$
where $\mathbf{Fc}$ and $\mathbf{Fv}$ denote Coulomb and viscous friction coefficients, respectively, and $\mathbf{B}$ is the bias term;
- Parameter matrix errors [42]
$$\boldsymbol{\Delta}_\mathbf{D} := \{\boldsymbol{\Delta}\mathbf{M}(\mathbf{q}), \boldsymbol{\Delta}\mathbf{C}(\mathbf{q}, \dot{\mathbf{q}}), \boldsymbol{\Delta}\mathbf{G}(\mathbf{q})\}.$$

Remark 3. *In addition to the approach in (10), alternative methods for friction modeling are also available. For instance, the Coulomb's friction plus linear viscous friction model [43] and friction models incorporating thermal and load dependencies [44], [45], among others, have been proposed. However, the non-parametric structure of GP provides an advantage in modeling, as it relies solely on the input and output signals, thereby overcoming the dependency on a specific parametric friction model.*

Considering all the aforementioned factors, the residual dynamics can be expressed as

$$\boldsymbol{\tau}_\Delta = \boldsymbol{\tau}_F(\mathbf{q}, \dot{\mathbf{q}}) + \boldsymbol{\tau}_D(\mathbf{q}, \dot{\mathbf{q}}, \ddot{\mathbf{q}}, \boldsymbol{\Delta}_\mathbf{D}), \quad (11)$$

where $\boldsymbol{\tau}_D(\cdot)$ denotes the torque resulting from measurement and modeling errors. The goal of residual dynamics learning is to establish the latent regression model

$$\boldsymbol{\psi}(\mathbf{q}, \dot{\mathbf{q}}, \ddot{\mathbf{q}}) = \boldsymbol{\tau}_\Delta(\mathbf{q}, \dot{\mathbf{q}}, \ddot{\mathbf{q}}) + \mathbf{W} : \mathbb{R}^{3n\times 1} \mapsto \mathbb{R}^{n\times 1}, \quad (12)$$

where each element of $\boldsymbol{\tau}_\Delta(\cdot)$ represents the residual dynamics of one joint of the manipulator; $\mathbf{W} \sim \mathcal{N}(\mathbf{0}, \boldsymbol{\Sigma}_\Delta)$ is an additive Gaussian white noise with covariance matrix $\boldsymbol{\Sigma}_\Delta$. $\boldsymbol{\psi}(\cdot)$ represents the measurement of the residual dynamics, collected by the measurement set

$$\boldsymbol{\Psi}_\mathcal{D} = [\boldsymbol{\psi}_1, \ldots, \boldsymbol{\psi}_N]^T,\ \boldsymbol{\psi}_i = [\psi_i^1, \ldots, \psi_i^n]^T \in \mathbb{R}^n, \quad (13)$$

which can also be regarded as a sample set drawn from a noisy Gaussian process and calculated by

$$\boldsymbol{\psi}_i = \boldsymbol{\tau}_{m,i} - \boldsymbol{\tau}_{EL,i}. \quad (14)$$

Note that, the offline learning of residual dynamics is conducted during the process where no contact occurs. The inputs of the regression model belong to a sample subspace of a continuous n-joint space as denoted by

$$\mathbf{Z}_\mathcal{D} = [\mathbf{z}_1, \ldots, \mathbf{z}_N]^T,\ \mathbf{z}_i = [\mathbf{q}_i, \dot{\mathbf{q}}_i, \ddot{\mathbf{q}}_i]^T \in \mathbb{R}^{3n}. \quad (15)$$

At each state point $\mathbf{z}_*$, the predicted value of the residual dynamics follows a Gaussian distribution, that is,

$$\mathbf{p}(\boldsymbol{\tau}_\Delta|\mathcal{D}, \mathbf{z}_*, \boldsymbol{\theta}) \sim \mathcal{N}(\boldsymbol{\tau}_\Delta; \boldsymbol{\mu}(\mathbf{z}_*), \boldsymbol{\Sigma}(\mathbf{z}_*)), \quad (16)$$

where the $\boldsymbol{\mu}(\mathbf{z}_*)$ and $\boldsymbol{\Sigma}(\mathbf{z}_*)$ are obtained according to (9).

Remark 4. *In practice scenarios, obtaining an accurate friction model is often unattainable due to the presence of various uncertainties. Consequently, traditional system identification methods that explicitly account for the joint friction torque are no longer suitable for this particular task [6], [43]. In contrast, the data-driven methods explored in this paper do not rely on the availability of an accurate mechanism model. In our approach, the unknown friction torque is treated as part of the residual dynamics, which can be learned from offline data using GPR.*

IEEE Transactions on Automation Science and Engineering (T-ASE) paper, presented at ICRA 2024, Yokohama, Japan.

B. EGP System Modeling

The EGP model is established based on a generalized momentum model derived from the nominal dynamic model (1). By utilizing the generalized momentum $\mathbf{p} \in \mathbb{R}^n$, the need for acceleration measurements, which can be heavily affected by noise, is eliminated. The generalized momentum can be represented as follows:

$$\mathbf{p} = \mathbf{M}(\mathbf{q})\dot{\mathbf{q}}. \tag{17}$$

The time evolution of $\mathbf{p}$ can be obtained by utilizing (1) and (3), yielding the following exression:

$$\begin{aligned}\dot{\mathbf{p}} &= \dot{\mathbf{M}}(\mathbf{q})\dot{\mathbf{q}} + \mathbf{M}(\mathbf{q})\ddot{\mathbf{q}} \\ &= \mathbf{C}^{\mathbf{T}}(\mathbf{q}, \dot{\mathbf{q}})\dot{\mathbf{q}} - \mathbf{G}(\mathbf{q}) + \boldsymbol{\tau}_m - \boldsymbol{\tau}_{ext} - \boldsymbol{\tau}_\Delta.\end{aligned} \tag{18}$$

By defining $\mathbf{x} := \mathbf{p} \in \mathbb{R}^n$ as the state vector, the generalized momentum model (18) can be expressed in state-space form as follows:

$$\dot{\mathbf{x}}(t) = \mathbf{A}\mathbf{x}(t) + \mathbf{B}\mathbf{u}(t) + \mathbf{D}_1\mathbf{d}_1(t) + \mathbf{D}_2\mathbf{d}_2(t), \tag{19}$$

with

$$\begin{aligned}\mathbf{u}(t) &:= \mathbf{C}^T(\mathbf{q}(t), \dot{\mathbf{q}}(t))\dot{\mathbf{q}}(t) - \mathbf{G}(\mathbf{q}(t)) + \boldsymbol{\tau}_m(t), \\ \mathbf{d}_1(t) &:= \boldsymbol{\tau}_{ext}(t), \quad \mathbf{d}_2(t) := \boldsymbol{\tau}_\Delta(t),\end{aligned} \tag{20}$$

where $\mathbf{u}(t) \in \mathbb{R}^n$ is regarded as the input vector; $\mathbf{d}_1 \in \mathbb{R}^n$ and $\mathbf{d}_2 \in \mathbb{R}^n$ are the additive disturbances. The system matrices in (19) are defined as: $\mathbf{A} = \mathbf{0}_{n\times n}$, $\mathbf{B} = \mathbf{I}_n$, $\mathbf{D}_1 = -\mathbf{I}_n$, and $\mathbf{D}_2 = -\mathbf{I}_n$. Note that the input $\mathbf{u}(t)$ is deterministic as the randomness in the control signal is absorbed by $\mathbf{d}_2(t)$ during the training process of GPs.

The discretized form of (19) is expressed as

$$\mathbf{x}_k = \boldsymbol{\Phi}_k\mathbf{x}_{k-1} + \mathbf{F}_k\mathbf{u}_k + \mathbf{E}_{1,k}\mathbf{d}_{1,k} + \mathbf{E}_{2,k}\mathbf{d}_{2,k}, \tag{21}$$

where the subscript $\cdot_k$ and $\cdot_{k-1}$ denote the matrices and vectors sampled at the discrete-time steps t_k and t_{k-1}, respectively. For time-invariant systems, the discretized system matrices are derived from the state transition matrix $\boldsymbol{\Phi}(t_{k-1}, t_k) = e^{\mathbf{A}(t_k - t_{k-1})}$.

The modeling of the EGP system based on the generalized momentum model comprises the following two components.

1) Modeling the additive disturbances $\mathbf{d}_1$ and $\mathbf{d}_2$: In practice, the unknown contact force $\mathbf{d}_1$ is time-varying. It is reasonable to assume that $\mathbf{d}_1$ is generated by the following exogenous dynamic system [26], [46]:

$$\boldsymbol{\omega}_k = \mathbf{S}_k\boldsymbol{\omega}_{k-1} + \mathbf{W}_{d,k-1}, \tag{22a}$$

$$\mathbf{d}_{1,k} = \mathbf{H}_k\boldsymbol{\omega}_k, \tag{22b}$$

where $\boldsymbol{\omega}_k \in \mathbb{R}^{nl}$ denotes the state variable of the force dynamic system; l is the order of the external torque; $\mathbf{S}_k \in \mathbb{R}^{nl\times nl}$ and $\mathbf{H}_k \in \mathbb{R}^{n\times nl}$ are coefficient matrices satisfying the condition that the pair $(\mathbf{S}_k, \mathbf{E}_{1,k}\mathbf{H}_k)$ is observable.

The noise term $\mathbf{W}_{d,k-1} \sim \mathcal{N}(\mathbf{0}, \boldsymbol{\Sigma}_{d,k-1})$ is utilized to characterize the uncertainty in the force dynamics. Obtaining precise knowledge of the covariance matrix $\boldsymbol{\Sigma}_{d,k-1}$ is typically challenging due to environmental variations and the unpredictable nature of contact forces. Therefore, in Section V-A, an online identification method will be introduced for $\boldsymbol{\Sigma}_{d,k-1}$.

Remark 5. *The exogenous dynamic system model (22) is capable of describing a wide range of contact forces, including unknown payloads, periodic interactions with known frequency but unknown magnitude, and viscoelastic contact forces. Generally, the contact force can be modeled as an l-order polynomial model with the corresponding system matrices:*

$$\begin{aligned}\mathbf{H}_k &= \begin{bmatrix}\mathbf{I}_{n\times n} & \mathbf{0}_{n\times n(l-1)}\end{bmatrix} \\ \mathbf{S}_k &= \begin{bmatrix}\mathbf{I}_{n(l-1)\times n} & (t_k - t_{k-1})\cdot\mathbf{I}_{n(l-1)} \\ \mathbf{0}_{n\times n} & \mathbf{I}_{n\times n(l-1)}\end{bmatrix}.\end{aligned} \tag{23}$$

Given the slowly time-varying characteristic of the contact force, the order l is typically small. In the case of a constant force, one has $l = 1$ and $\mathbf{S}_k$ degenerates to the identity matrix.

The residual dynamics $\mathbf{d}_2$ is learned offline using GPR, as explained in Section IV-A. The prediction model presented in (16) can be reformulated as follows:

$$\mathbf{d}_{2,k} = \boldsymbol{\mu}_{\Delta,k}(\mathbf{z}_*) + \mathbf{W}_{\Delta,k}(\mathbf{z}_*), \tag{24}$$

where $\boldsymbol{\mu}_{\Delta,k}(\mathbf{z}_*) \in \mathbb{R}^n$ represents the mean value of the predictive residual dynamics; $\mathbf{W}_{\Delta,k}(\mathbf{z}_*) \sim \mathcal{N}(\mathbf{0}, \boldsymbol{\Sigma}_{\Delta,k}(\mathbf{z}_*))$ denotes Gaussian noise with a state-dependant covariance matrix $\boldsymbol{\Sigma}_{\Delta,k}(\mathbf{z}_*)$. Note that the uncertainties in the learned residual dynamic model are incorporated in $\boldsymbol{\Sigma}_{\Delta,k}(\mathbf{z}_*)$, which is updated at each sampling instant. Specifically, $\boldsymbol{\Sigma}_{\Delta,k}(\mathbf{z}_*) = \mathrm{diag}(\sigma_\Delta^1(\mathbf{z}_*), \ldots, \sigma_\Delta^{\mathrm{n}}(\mathbf{z}_*))$ is a diagonal matrix as the residual dynamics of each joint are trained independently.

2) Establishing the virtual measurement equation: In traditional approaches, the contact force is incorporated as an augmented state in the dynamic equation of the manipulator, resulting in an increased state dimension. However, in what follows, a virtual measurement equation will be introduced, establishing a direct relationship between the contact force and the measured signals without expanding the dimension.

In most manipulator systems, the generalized momentum $\mathbf{x}_k$ in (21) is measurable. Therefore, we have $\mathbf{y}_k = \mathbf{p}_k$. By defining the virtual measurement signal as

$$\boldsymbol{\zeta}_k^* := \mathbf{y}_k - \boldsymbol{\Phi}_k\mathbf{y}_{k-1} - \mathbf{F}_k\mathbf{u}_k - \mathbf{E}_{2,k}\boldsymbol{\mu}_{\Delta,k}, \tag{25}$$

and rearranging (21) and (22), the following EGP model with a virtual measurement equation for the contact force can be obtained:

$$\begin{cases}\boldsymbol{\omega}_k = \mathbf{S}_k\boldsymbol{\omega}_{k-1} + \mathbf{W}_{d,k-1}, \\ \boldsymbol{\zeta}_k^* = \mathbf{E}_{1,k}\mathbf{H}_k\boldsymbol{\omega}_k + \boldsymbol{\nu}_k,\end{cases} \tag{26}$$

where $\boldsymbol{\nu}_k \sim \mathcal{N}(0, \boldsymbol{\Sigma}_{\nu,k})$ is the virtual measurement noise, which is expressed as

$$\boldsymbol{\nu}_k = \mathbf{E}_{2,k}\mathbf{W}_{\Delta,k}, \tag{27}$$

with the covariance matrix given by

$$\boldsymbol{\Sigma}_{\nu,k} = \mathbf{E}_{2,k}\boldsymbol{\Sigma}_{\Delta,k}. \tag{28}$$

By referring to equation (26), it becomes apparent that the virtual measurement equation allows for the utilization of information from both the physical mechanism of the robot manipulator and the data-driven model acquired through GPR. Additionally, note that the virtual measurement noise,

IEEE Transactions on Automation Science and Engineering (T-ASE) paper, presented at ICRA 2024, Yokohama, Japan.

characterized by state-dependent covariance matrices, effectively incorporates the uncertainties present in the learning of residual dynamics as well as the torque measurement noise.

V. Force Estimation Using the GPADKF

In this section, a GPADKF algorithm will be developed to tackle the problem of estimating contact forces. This algorithm takes into consideration the unknown covariance matrices of the contact force model and the multi-source disturbances.

A. Algorithm design

As mentioned in Section IV-B, the contact force (26) is a Gaussian stochastic system with an unknown process noise covariance matrix $\mathbf{\Sigma}_{d,k-1}$, resulting that the covariance matrix associated with the one-step prediction of Kalman filter (KF), denoted as $\mathbf{P}_{k|k-1}$, will also be unknown. In the Bayesian estimation framework, the joint posterior PDF denoted as $p(\boldsymbol{\omega}_k, \mathbf{P}_{k|k-1}|\boldsymbol{\zeta}^*_{1:k})$ needs to be computed. To accomplish this, the VB inference [10] technique is employed to approximate the joint prior PDF efficiently:

$$p(\boldsymbol{\omega}_k, \mathbf{P}_{k|k-1}|\boldsymbol{\zeta}^*_{1:k}) \approx q(\boldsymbol{\omega}_k)q(\mathbf{P}_{k|k-1}), \tag{29}$$

where $q(\boldsymbol{\omega}_k)$, $q(\mathbf{P}_{k|k-1})$ is given by

$$\begin{aligned}\{q(\boldsymbol{\omega}_k), q(\mathbf{P}_{k|k-1})\} = \operatorname{argmin}\ & KL(q(\boldsymbol{\omega}_k) \\ & \times q(\mathbf{P}_{k|k-1})||p(\boldsymbol{\omega}_k, \mathbf{P}_{k|k-1}|\boldsymbol{\zeta}^*_{1:k})),\end{aligned} \tag{30}$$

where $KL(q(\cdot)||p(\cdot)) := \int q(\cdot)\ln\frac{q(\cdot)}{p(\cdot)}dx$ is the Kullback-Leibler divergence between two PDFs $q(\cdot)$ and $p(\cdot)$. The optimal solution for (30) is

$$\ln\ q(\xi) = \mathbb{E}_{\Omega^{(-\xi)}}[\ln\ p(\Omega, \boldsymbol{\zeta}^*_{1:k})] + c_\xi, \tag{31}$$

where $\Omega := \{\boldsymbol{\omega}_k, \mathbf{P}_{k|k-1}\}$; ξ is an arbitrary element of the set Ω; $\Omega^{(-\xi)}$ denotes the remaining set after ξ has been removed from Ω; c_ξ denotes a constant with respect to ξ.

The joint PDF is computed using the conditional independence properties as [47]

$$\begin{aligned}p(\Omega, \boldsymbol{\zeta}^*_{1:k}) = & p(\boldsymbol{\zeta}^*_k|\omega_k, \mathbf{\Sigma}_{\nu,k})p(\boldsymbol{\omega}_k|\boldsymbol{\zeta}^*_{1:k-1}, \mathbf{P}_{k|k-1}) \\ & \times p(\mathbf{P}_{k|k-1}|\boldsymbol{\zeta}^*_{1:k-1})p(\mathbf{\Sigma}_{\nu,k}|\boldsymbol{\zeta}^*_{1:k-1})p(\boldsymbol{\zeta}^*_{1:k-1}),\end{aligned} \tag{32}$$

where $p(\mathbf{\Sigma}_{\nu,k}|\boldsymbol{\zeta}^*_{1:k-1}) \equiv 1$ is the uninformative prior distribution; $p(\boldsymbol{\omega}_k|\boldsymbol{\zeta}^*_{1:k-1}, \mathbf{P}_{k|k-1})$ and $p(\boldsymbol{\zeta}^*_k|\boldsymbol{\omega}_k, \mathbf{\Sigma}_{\nu,k})$ are the one-step predicted PDF and the likelihood PDF respectively, both of which are Gaussian, that is,

$$p(\boldsymbol{\omega}_k|\boldsymbol{\zeta}^*_{1:k-1}, \mathbf{P}_{k|k-1}) = \mathcal{N}(\boldsymbol{\omega}_k; \hat{\boldsymbol{\omega}}_{k|k-1}, \mathbf{P}_{k|k-1}), \tag{33}$$

$$p(\boldsymbol{\zeta}^*_k|\boldsymbol{\omega}_k, \mathbf{\Sigma}_{\nu,k}) = \mathcal{N}(\boldsymbol{\zeta}^*_k; \mathbf{E}_{1,k}\mathbf{H}\boldsymbol{\omega}_k, \mathbf{\Sigma}_{\nu,k}), \tag{34}$$

where the covariance matrix $\mathbf{\Sigma}_{\nu,k}$ is updated using GP prediction (16) and (28); $\hat{\boldsymbol{\omega}}_{k|k-1}$ and $\mathbf{P}_{k|k-1}$ in (33) are the predictive mean and predictive error covariance matrix (PECM) of the contact force, which are derived as

$$\hat{\boldsymbol{\omega}}_{k|k-1} = \mathbf{S}_k\hat{\boldsymbol{\omega}}_{k-1|k-1}, \tag{35}$$

$$\mathbf{P}_{k|k-1} = \mathbf{S}_k\mathbf{P}_{k-1|k-1}\mathbf{S}_k^T + \mathbf{\Sigma}_{d,k-1}. \tag{36}$$

In (36), $\mathbf{P}_{k|k-1}$ is unknown and needs to be estimated along with the contact force. In the VB framework, the following inverse Wishart PDF is chosen as its prior distribution [48]:

$$p(\mathbf{P}_{k|k-1}|\boldsymbol{\zeta}^*_{1:k-1}) = \mathcal{IW}(\mathbf{P}_{k|k-1}; \lambda_{k|k-1}, \Upsilon_{k|k-1}), \tag{37}$$

where $\mathcal{IW}(\cdot; \lambda_{k|k-1}, \Upsilon_{k|k-1})$ denotes the inverse Wishart PDF with the degrees of freedom parameter $\lambda_{k|k-1}$ and the positive definite symmetric inverse scale matrix $\Upsilon_{k|k-1} \in \mathbb{R}^{\eta\times\eta}$, with η represents the dimension.

Substituting (33), (34) and (37) into (32), yields

$$\begin{aligned}\ln\ p(\Omega, \boldsymbol{\zeta}^*_{1:k}) = & -\frac{1}{2}\mathrm{tr}(\lambda_{k|k-1}\mathbf{P}^{-1}_{k|k-1}) + c_\Omega \\ & -\frac{1}{2}(\boldsymbol{\zeta}^*_k - \mathbf{E}_{1,k}\mathbf{H}_k\boldsymbol{\omega}_k)^T\mathbf{\Sigma}^{-1}_{\nu,k}(\boldsymbol{\zeta}^*_k - \mathbf{E}_{1,k}\mathbf{H}_k\boldsymbol{\omega}_k) \\ & -\frac{1}{2}\ln|\mathbf{\Sigma}_{\nu,k}| - \frac{1}{2}(\eta + \lambda_{k|k-1} + 2)\ln|\mathbf{P}_{k|k-1}| \\ & -\frac{1}{2}(\hat{\boldsymbol{\omega}}_k - \hat{\boldsymbol{\omega}}_{k|k-1})^T\mathbf{P}^{-1}_{k|k-1}(\hat{\boldsymbol{\omega}}_k - \hat{\boldsymbol{\omega}}_{k|k-1}),\end{aligned} \tag{38}$$

where $\mathrm{tr}(\cdot)$ denotes the trace operator, and the constant c_Ω is dependent on Ω.

Letting $\xi = \mathbf{P}_{k|k-1}$, the approximate distribution $q(\mathbf{P}_{k|k-1})$ can be updated according to (31) and (38) as

$$\begin{aligned}\ln\ q^{(i+1)}(\mathbf{P}_{k|k-1}) = & -\frac{1}{2}(\eta + \lambda_{k|k-1} + 2)\ln\ |\mathbf{P}_{k|k-1}| \\ & -\frac{1}{2}\mathrm{tr}((\alpha^{(i)}_k + \Upsilon_{k|k-1})\mathbf{P}^{-1}_{k|k-1}) + c_p,\end{aligned} \tag{39}$$

where the subscript (i) denotes the ith iteration, c_p is a constant, and $\alpha^{(i)}_k$ is given by

$$\begin{aligned}\alpha^{(i)}_k &= \mathbb{E}^{(i)}[(\hat{\boldsymbol{\omega}}_k - \hat{\boldsymbol{\omega}}_{k|k-1})(\hat{\boldsymbol{\omega}}_k - \hat{\boldsymbol{\omega}}_{k|k-1})^T] \\ &= \mathbf{P}^{(i)}_{k|k} + (\hat{\boldsymbol{\omega}}^{(i)}_{k|k} - \hat{\boldsymbol{\omega}}_{k|k-1})(\hat{\boldsymbol{\omega}}^{(i)}_{k|k} - \hat{\boldsymbol{\omega}}_{k|k-1})^T.\end{aligned} \tag{40}$$

According to (39), $q^{(i+1)}(\mathbf{P}_{k|k-1})$ can be updated as

$$q^{(i+1)}(\mathbf{P}_{k|k-1}) = \mathcal{IW}(\mathbf{P}_{k|k-1}; \lambda^{(i+1)}_{k|k-1}, \Upsilon^{(i+1)}_{k|k-1}), \tag{41}$$

with

$$\lambda^{(i+1)}_{k|k-1} = \lambda_{k|k-1} + 1, \tag{42}$$

$$\Upsilon^{(i+1)}_{k|k-1} = \alpha^{(i)}_k + \Upsilon_{k|k-1}, \tag{43}$$

Letting $\xi = \omega_k$, $\ln\ q^{(i+1)}(\omega_k)$ can be calculated in a similar fashion as

$$\begin{aligned}\ln\ q^{(i+1)}(\omega_k) = & -\frac{1}{2}(\hat{\boldsymbol{\omega}}_{k|k} - \hat{\boldsymbol{\omega}}_{k|k-1})^T\mathbb{E}^{(i+1)}[\mathbf{P}^{-1}_{k|k-1}] \\ & \times (\hat{\boldsymbol{\omega}}_{k|k} - \hat{\boldsymbol{\omega}}_{k|k-1}) + c_\omega,\end{aligned} \tag{44}$$

where c_ω is a constant. Based on (41) and the property in [48], one has

$$\mathbb{E}^{(i+1)}[\mathbf{P}^{-1}_{k|k-1}] = (\lambda^{(i+1)}_{k|k-1} - \eta - 1)(\Upsilon^{(i+1)}_{k|k-1})^{-1}. \tag{45}$$

Denoting

$$\hat{\mathbf{P}}^{(i+1)}_{k|k-1} = \mathbb{E}^{(i+1)}[\mathbf{P}^{-1}_{k|k-1}]^{-1}, \tag{46}$$

the approximate posterior distribution of ω_k can be updated as

$$q^{(i+1)}(\boldsymbol{\omega}_k) \sim \mathcal{N}(\boldsymbol{\omega}_k; \hat{\boldsymbol{\omega}}^{(i+1)}_{k|k}, \mathbf{P}^{(i+1)}_{k|k}),$$

IEEE Transactions on Automation Science and Engineering (T-ASE) paper, presented at ICRA 2024, Yokohama, Japan.

with

$$\mathbf{K}_k^{(i+1)} = \hat{\mathbf{P}}_{k|k-1}^{(i+1)}(\mathbf{E}_{1,k}\mathbf{H}_k)^T \times [\mathbf{E}_{1,k}\mathbf{H}_k\hat{\mathbf{P}}_{k|k-1}^{(i+1)}(\mathbf{E}_{1,k}\mathbf{H}_k)^T + \mathbf{\Sigma}_{\nu,k}]^{-1}, \tag{47}$$

$$\hat{\boldsymbol{\omega}}_{k|k}^{(i+1)} = \hat{\boldsymbol{\omega}}_{k|k-1} + \mathbf{K}_k^{(i+1)}({\boldsymbol{\zeta}^*}_k - \mathbf{E}_{1,k}\mathbf{H}_k\hat{\boldsymbol{\omega}}_{k|k-1}), \tag{48}$$

$$\mathbf{P}_{k|k}^{(i+1)} = \hat{\mathbf{P}}_{k|k-1}^{(i+1)} - \mathbf{K}_k^{(i+1)}\mathbf{E}_{1,k}\mathbf{H}_k\hat{\mathbf{P}}_{k|k-1}^{(i+1)}. \tag{49}$$

Note that the contact force and the PECM have been jointly estimated using VB, and the virtual measurement noise is updated utilizing the GP model. The comprehensive GPADKF algorithm is presented in **Algorithm 1**. Here, M is the maximum number of iterations for the VB procedure.

Remark 6. *The proposed GPADKF algorithm has the advantage of not affecting the overall structure of the closed-loop control system. This flexibility makes it well-suited for replacing the force estimation module in existing control frameworks. Here are three typical integration scenarios: 1) In the CHADC framework [31], the GPADKF can serve as a DO for real-time compensation. The computed torque controller can be employed as the inner-loop controller to ensure accurate position tracking. 2) As a KF-based method, the proposed GPADKF method can also be integrated into the stochastic model predictive control framework, providing real-time force information [8]. 3) The proposed method can be extended to multi-sensor fusion system, where elegant distributed filtering and control methods can be adopted [49], [50].*

Remark 7. *The proposed GPADKF improves upon the KF-based method by incorporating additional GP and VB modules for residual dynamics learning and process noise covariance identification, respectively. Consequently, the stability analysis of GPADKF can be simplified to a KF stability problem involving inaccurate noise covariance matrices. The mean stability of the filter can be established based on Theorem 3 in [13] under this condition. Regarding the convergence of error covariance matrices estimation, it should be noted that the use of incorrect Riccati equations, resulting from inaccurate noise covariance matrices, can prevent the estimated covariance from converging to the true value. Quantifying the error between the estimated and true covariance matrices caused by inaccurate noise covariance matrices is challenging. However, practical approaches such as consistency checks and fuzzy logic methods [51] can be employed to detect filter divergence. Additionally, the application of non-Gaussian stochastic systems theory holds promise in addressing the imprecise characterization of noise models [52].*

Algorithm 1 The GPADKF algorithm

TRAIN ($\mathbf{GP}$) $\mathrm{p}(\boldsymbol{\tau}_\Delta|\mathcal{D}, \mathbf{z}_*, \boldsymbol{\theta})$
Inputs: Dataset $\mathcal{D} = \{\mathbf{Z}_\mathcal{D}, \mathbf{\Psi}_\mathcal{D}\}, \mathbf{z}_i = [\mathbf{q}_i, \dot{\mathbf{q}}_i, \ddot{\mathbf{q}}_i]^T$
Train:
Initialization: $\boldsymbol{\theta}_0 = [\sigma_{f,1,0}^2, \ldots, \sigma_{f,n,0}^2, \sigma_{n,0}^2, l_{1,0}, \ldots, l_{ND_z,0}]$
Mean function: $m(\cdot)$
Covariance function: $k(\cdot,\cdot)$
Train GP: $\boldsymbol{\theta} = \operatorname{argmin} -\ln \mathrm{p}(\mathbf{\Psi}_\mathcal{D}|\mathbf{Z}_\mathcal{D}, \boldsymbol{\theta})$
Outputs: $\boldsymbol{\theta}, \mathcal{D} = \{\mathbf{Z}_\mathcal{D}, \mathbf{\Psi}_D\}$

ESTIMATION ($\mathbf{ADKF}$) $\hat{\mathbf{F}}_{ext,k}$ at k-step
Inputs: $\hat{\boldsymbol{\omega}}_{k-1|k-1}, \mathbf{P}_{k-1|k-1}, \mathbf{S}_k, \mathbf{E}_{1,k}, \mathbf{\Sigma}_{d,k-1}, \mathbf{\Sigma}_{v,k}$ $\mathbf{H}_k, \mathbf{\Phi}_k, \mathbf{F}_k, \mathbf{E}_{2,k}, \mathbf{y}_k, \mathbf{y}_{k-1}, \mathbf{u}_k, \mathbf{z}_*, \mathcal{D}, \boldsymbol{\theta}, \eta, \tau, M, \mathbf{\Sigma}_{v,k-1},$
Time update:
$\hat{\boldsymbol{\omega}}_{k|k-1} = \mathbf{S}_k\hat{\boldsymbol{\omega}}_{k-1|k-1}$
$\mathbf{P}_{k|k-1} = \mathbf{S}_k\mathbf{P}_{k-1|k-1}\mathbf{S}_k^T + \mathbf{\Sigma}_{d,k-1}$
Virtual EGP measurement update:
GP mean: $\boldsymbol{\mu}_{\Delta,k}(\mathbf{z}_*) = m(\mathbf{z}_*) + \mathbf{k}_{\mathbf{z}_*\mathbf{z}_D}^T K^{-1}(\mathbf{\Psi}_D - \mathbf{m}(\mathbf{z}_D))$
GP covariance: $\mathbf{\Sigma}_{\Delta,k}(\mathbf{z}_*) = k_{\mathbf{z}_*\mathbf{z}_*} - \mathbf{k}_{\mathbf{z}_*\mathbf{z}_D}^T K^{-1}\mathbf{k}_{\mathbf{z}_*\mathbf{z}_D}$
Virtual measurement: $\boldsymbol{\zeta}_k^* := \mathbf{y}_k - \mathbf{\Phi}_k\mathbf{y}_{k-1} - \mathbf{F}_k\mathbf{u}_k - \mathbf{E}_{2,k}\boldsymbol{\mu}_{\Delta,k}$
Virtual covariance: $\mathbf{\Sigma}_{\nu,k} = \mathbf{E}_{2,k}\mathbf{\Sigma}_{\Delta,k} + \mathbf{\Sigma}_{v,k} - \mathbf{\Phi}_k\mathbf{\Sigma}_{v,k-1}$
Variational measurement update:
Initialization: $\hat{\boldsymbol{\omega}}_{k|k}^{(0)} = \hat{\boldsymbol{\omega}}_{k|k-1}(35), \mathbf{P}_{k|k}^{(0)} = \mathbf{P}_{k|k-1}(36),$ $\lambda_{k|k-1} = \eta + \tau + 1, \Upsilon_{k|k-1} = \tau\mathbf{P}_{k|k-1},$
for $i = 0 : M-1$
Update: $q^{(i+1)}(\mathbf{P}_{k|k-1}) = \mathcal{IW}(\mathbf{P}_{k|k-1}; \lambda_{k|k-1}^{(i+1)}, \Upsilon_{k|k-1}^{(i+1)})$ given $q^{(i)}(\boldsymbol{\omega}_k)$:
Compute: $\alpha_k^{(i)}$ (40), $\lambda_{k|k-1}^{(i+1)}$ (42), $\Upsilon_{k|k-1}^{(i+1)}$ (43)
Update: $q^{(i+1)}(\boldsymbol{\omega}_k) = \mathcal{N}(\boldsymbol{\omega}_k; \hat{\boldsymbol{\omega}}_{k|k}^{(i+1)}, \mathbf{P}_{k|k}^{(i+1)})$ given $q^{(i+1)}(\mathbf{P}_{k|k-1})$:
Compute: $\mathbb{E}^{(i+1)}[\mathbf{P}_{k|k-1}^{-1}]$ (45), $\hat{\mathbf{P}}_{k|k-1}^{(i+1)}$(46), $\mathbf{K}_k^{(i+1)}$ (47), $\hat{\boldsymbol{\omega}}_{k|k}^{(i+1)}$ (48), $\mathbf{P}_{k|k}^{(i+1)}$ (49)
end for
$\hat{\boldsymbol{\omega}}_k = \hat{\boldsymbol{\omega}}_{k|k}^{(M)}, \mathbf{P}_{k|k} = \mathbf{P}_{k|k}^{(M)}, \lambda_k = \lambda_{k|k-1}^{(M)}, \Upsilon_k = \Upsilon_{k|k-1}^{(M)}$
Outputs: $\hat{\boldsymbol{\omega}}_{k|k}, \mathbf{P}_{k|k}, \hat{\mathbf{d}}_{1,k} = \mathbf{H}_k\hat{\boldsymbol{\omega}}_{k|k}, \hat{\mathbf{F}}_{ext,k} = \mathbf{J}\hat{\mathbf{d}}_{1,k}$

B. Numerical simulation

To evaluate the effectiveness of the proposed GPADKF method, Monte Carlo simulations are conducted. In these simulations, the torque on each joint follows a Gaussian distribution with a constant mean and a standard deviation (SD) of 0.01 N·m. The performance of the proposed EGP model compensator is verified in a scenario with constant contact force while according for uncertainties. The injected uncertainties include residual dynamics, with a relative modeling error of 10% in the mass of each link, and measurement noises with zero mean and an SD of 0.01 N·m. The sampling interval is set to 0.005s. For training data of the residual dynamics, 30 sets of finite Fourier series trajectories are randomly generated in the joint space under the contact-free scenario. The manipulator follows a linear segment with a parabolic blend (LSPB) trajectory within two-second interval. The torque exerted on each manipulator link is set to be piecewise constant, with value of $[0, -2, -1]$ N·m from 0s to 1s and $[0, -3, -1.5]$ N·m from 1s to 2s.

The performance of the GPADKF method is compared to several traditional techniques, including DKF [12], GMO [22], NDO [27], DO-based reaction force observer (RFO) [25], and the EDKF. The EDKF is a variant of DKF that incorporates a residual dynamics compensator, utilizing only the mean value

IEEE Transactions on Automation Science and Engineering (T-ASE) paper, presented at ICRA 2024, Yokohama, Japan.

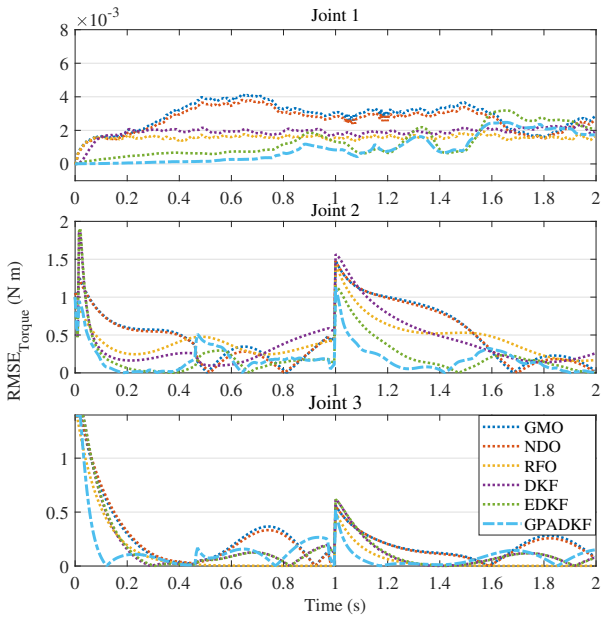

Figure 2. The RMSEs of torque estimates under the measurement noises and the residual dynamics.

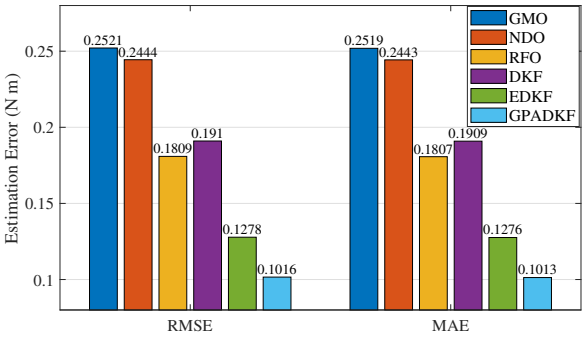

Figure 3. The averaged RMSEs and MAEs of torque estimates.

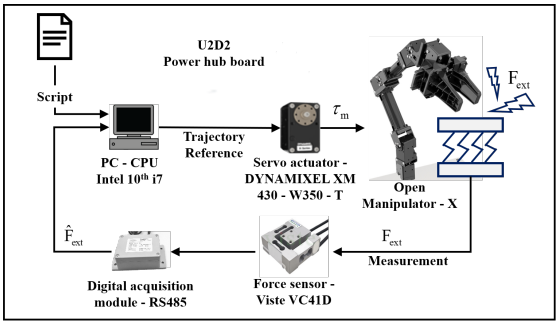

(a)

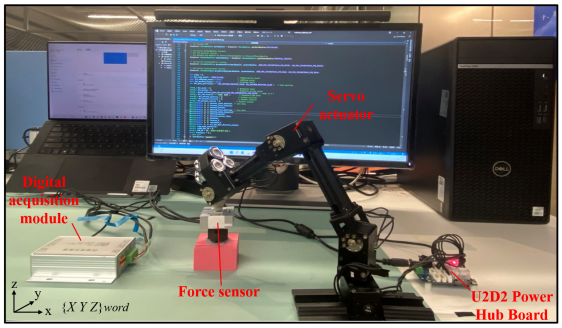

(b)

Figure 4. Experiment setup. (a).The schematic diagram of the robotics system. (b). The experiment platform.

Table II
D-H PARAMETERS OF THE OPENMANIPULATOR

Link	α	a	d	θ
1	$\frac{\pi}{2}$	0	0.077	q_1
2	0	0.1304	0	q_2
3	0	0.124	0	q_3

predicted by the GP for compensation. The gain matrices for NDO, GMO, and RFO are set to $\mathrm{diag}(10, 10, 10)$.

The root mean square errors (RMSEs) of the force estimation for the three joints are shown in Fig. 2. It can be observed that both EDKF and GPADKF exhibit smaller steady-state errors due to the residual dynamics compensation. Moreover, GPADKF demonstrates faster convergence compared to EDKF, thanks to more precise quantification of uncertainties in residual dynamics learning. The averaged RMSEs (ARMSEs) and the mean absolute errors (MAEs) are illustrated in Fig. 3. Notably, the proposed GPADKF achieves the lowest ARMSEs and MAEs among all the methods. This highlights the effectiveness of the proposed scheme in compensating for residual dynamics and attenuating noise.

VI. Experimental Results

A. Experimental Setup

The algorithms under evaluation are implemented on a 3-DoF serial OpenManipulator, depicted in Fig. 4. Each joint is equipped with the DYNAMIXEL XM-430-W350-T servo actuator, which has a stall torque of 4.1 N·m. During operation, all joints provide feedback on joint position, velocity, and motor current. The joint torque is determined using the N-T curve, also known as the performance graph. To ensure accurate torque measurement, three 100g weights are symmetrically placed on Link3. This arrangement ensure that the current measurement falls within the linear range of the N-T curves. The Denavit-Hartenberg (D-H) parameters of the manipulator are listed in Table II.

The experiment consists of two groups. The first group aims to validate the effectiveness of the EGP model in real interaction scenarios by validating the residual dynamic model and quantifying model uncertainties. The second group is designed to compare the GPADKF with other state-of-the-art force estimation methods.

B. Data Acquisition

The experimental validation utilizes a dataset collected at a sampling frequency of 1000Hz. The dataset comprises tuples of position, velocity, acceleration (obtained through numerical differentiation of the velocity curve), and torque (derived from

IEEE Transactions on Automation Science and Engineering (T-ASE) paper, presented at ICRA 2024, Yokohama, Japan.

motor current) data for all joints at each time step. Position, velocity, and acceleration are selected as the features.

To ensure generalization, the generated data must encompass the entire workspace and exhibit sufficient richness. To achieve this, additional informative data is artificially generated, requiring persistent excitation and more dynamic changes within a smaller dataset. Consequently, the data for model learning is sampled from twelve $eighth$-order Fourier series trajectories generated within each permissible joint space. The trajectory parameters are adjusted to fully cover the entire workspace. The complete dataset consists of 47,145 samples, with 38,078 samples allocated for training and 9,067 samples for testing. The test and training datasets are randomly partitioned.

The nominal inverse dynamics of the robot manipulator are generated using Matlab/Robotic System Toolbox, incorporating the physical parameters from the official manual of the OpenManipulator with adjusted masses. The GP learning process is conducted using the GPML Toolbox.

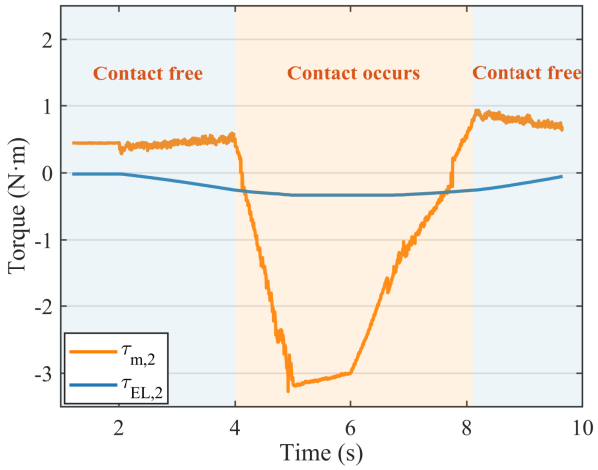

Figure 5. The residual dynamics test of the joint-2 in the real contact scenarios.

C. Validation of the EGP Model

In this subsection, the effectiveness of the EGP model in learning and compensating for the residual dynamics will be evaluated.

The residual dynamics compensation term, learned through GP, is critical in the EGP model. To prevent overfitting and mitigate computational complexity, the GP is implemented with a zero mean and SE covariance function that incorporates automatic relevance determination (ARD). For computationally feasible force estimation tasks, a sparse GP approximation is employed. The apxSparse function is utilized to approximate the GP posterior, optimizing the inducing points through power expectation propagation during the Bayesian inference process for covariance matrix approximation [53] [54].

1) Residual dynamics testing in the real interactive scenarios: We assess the residual dynamics in real interactive scenarios by conducting a contact experiment between the robotic manipulator and an EVA foam block. Fig. 5 displays the total joint torque and the nominal torque of joint two. In the operation, the end-effector remains in contact with the foam block from 4s to 8.21s, while the contact-free phases span from 1s to 4s and from 8.21s to 9.8s. In an ideal case with no residual dynamics, the total joint torque during the contact-free phase should be zero. However, the actual joint torque $\boldsymbol{\tau}_{m,2}$ consists of both the residual dynamics $\boldsymbol{\tau}\Delta, 2$ and the nominal torque $\boldsymbol{\tau}_{EL,2}$.

2) Evaluation of the EGP model trained with and without acceleration: The RMSE is adopted as the performance metric to quantify the disparity between the predicted joint torque by EGP model and the actual joint torque, that is,

$$\text{RMSE} = \mathbb{E}[(\boldsymbol{\tau}_m - (\boldsymbol{\tau}_{EL} + \hat{\boldsymbol{\tau}}_\Delta))^2].$$

As illustrated in Fig. 6, the test error of the EGP model is represented by the two-color box lines, where one model is trained with acceleration while the other is trained without acceleration. The comparison between the two models reveals no noticeable disparities in terms of training accuracy and the distribution of test error. Consequently, for subsequent steps, the EGP model is solely trained using position and velocity.

Remark 8. *Typically, including acceleration in the training of a dynamic model leads to improved accuracy. However, in this specific task, the negligible impact of acceleration on residual dynamics learning can be attributed to two factors: 1) the minor differences in the inertia matrix, and 2) the assumption of low-speed motion. Generally, when there is a mismatch between the actual and inaccurate inertia matrix, non-collocated disturbances can arise, potentially degrading force estimation performance, particularly in high-speed scenarios.*

Remark 9. *Notably, when comparing joint 1 and joint 3, the test error outliers in joint 2 exhibit a more pronounced concentration around the median. This suggests that low-quality training data may have contributed to these outliers. Specifically, joint 2 has a wider range of motion during the data collection, allowing for the collection of a more diverse dataset. Consequently, training for joint 2 is less affected by the nonlinear dead zone present in the mechanical structure.*

3) The uncertainty of the EGP model: A key advantage of the EGP model is its ability to provide both the mean and the uncertainty (variance) of the predictions. The three-dimensional prediction of the EGP model on the test dataset is presented in Fig. 7.

To enhance clarity and conciseness, we extract points at regular intervals from the prediction results and display them in Figure 7. The performance of the selected portion of the prediction results is comparable to the rest. The performance index for the uncertainty of the EGP model is the Acc, which represents the percentage of true values falling within the 3-σ bound, that is,

$$\text{Acc} = \frac{\sum_{i=1}^{n} \text{if}(|\hat{\tau}_\Delta(i) - \tau_\Delta(i)| \leq 3\sigma)}{n} \times 100\%.$$

Figure 7 illustrates that the true values align closely with the predictions, with the majority falling within the confidence

IEEE Transactions on Automation Science and Engineering (T-ASE) paper, presented at ICRA 2024, Yokohama, Japan.

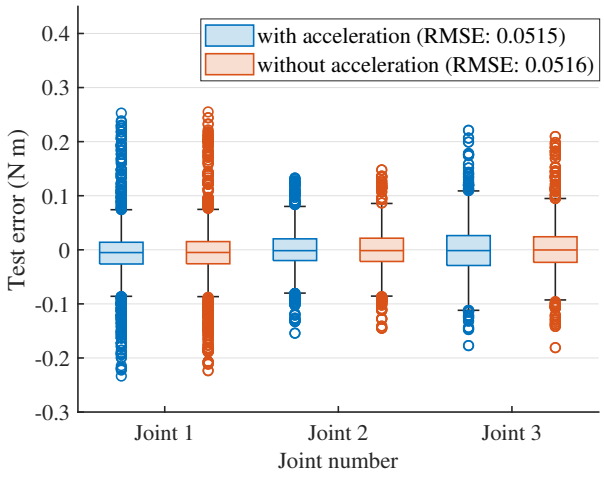

Figure 6. The two-color box lines illustrate the comparison between EGP models trained with and without acceleration. The middle line within each box represents the mean value, while the hollow circle dots indicate outliers.

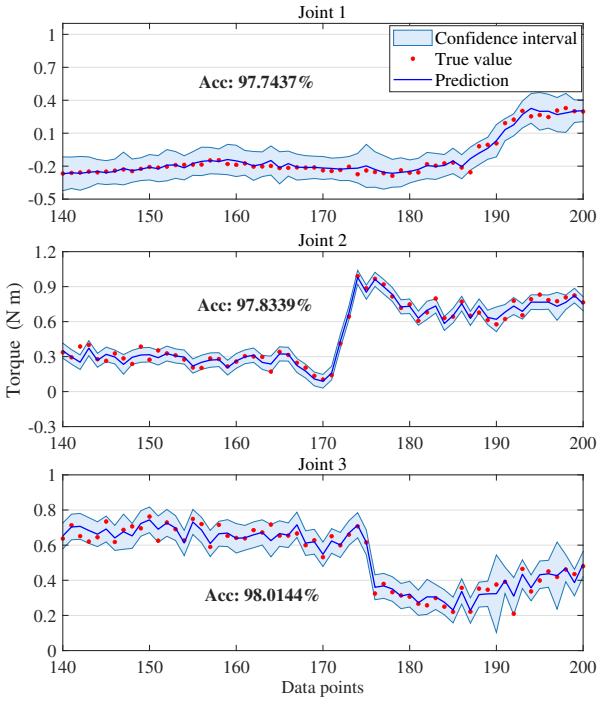

Figure 7. The joint torque predictions of the EGP model. In each subplot, sapphire blue solid lines denote the predicted torques of the EGP model, red dots representing the true values, and the light blue shaded area indicating the 95% confidence interval of the predictions.

interval. The GP model's uncertainty quantification achieves an accuracy of 97.7%.

In conclusion, the experimental results affirm the EGP model's efficacy in accurately predicting residual dynamics and quantifying uncertainty.

D. Contact Force Estimation Test

In this subsection, the proposed GPADKF method is validated in two real contact scenarios: 1) The first experiment

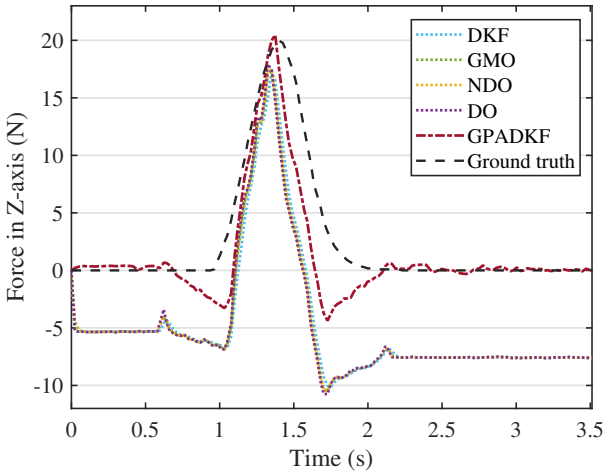

Figure 8. Contact force estimation result in Z-axis under a dynamic contact scenario.

evaluates the accuracy of the proposed method with residual dynamics compensation for dealing with inaccurate manipulator models. The GPADKF is compared against other methods without the residual dynamics compensation (DKF [12], GMO [22], NDO [27], and RFO [25]) as well as the ground truth. 2) The second experiment verifies the effect of VB (part of GPADKF) with inaccurate noise covariance matrices in the contact force model. Unlike existing DKF-based methods, GPADKF utilizes GP and VB to compute the gain based on online-identified noise covariance matrices. Since their gains are automatically calculated within the unified KF framework, The three DKF-based methods (DKF, EDKF, and GPADKF) are compared as a group under a constant force estimation scenario. Both experiments are conducted using the experimental platform introduced in Section V-A (see Fig. 4).

In the first experiment, the OpenManipulator is controlled to simulates button pressing by following a trajectory and making perpendicular contact with a force sensor fixed on the ground. This dynamic contact scenario consists of five stages: stillness, downward movement, contact, upward movement, and stillness. The force estimation results are presented in Fig. 8, with the ground truth obtained from a highly accurate force sensor. The initial force estimates for all five methods are set to zero.

As depicted in Fig. 8, the GPADKF outperforms all other methods in terms of the RMSE of contact force estimation, thanks to its accurate EGP model with residual dynamics compensation. Furthermore, the improvement in accuracy of the EGP model is more pronounced during the static state compared to the motion stages.

In the second experiment, three DKF-based methods are compared under a constant contact force scenario. The OpenManipulator is controlled to track a fixed-point trajectory, guaranteeing a constant contact force on the end-effector. The process noise and measurement noise covariance matrices are identical for DKF and EDKF. The initial process noise covariance matrix of GPADKF is also the same as those of the two comparison methods.

IEEE Transactions on Automation Science and Engineering (T-ASE) paper, presented at ICRA 2024, Yokohama, Japan.

Table III
EVALUATION OF THE FORCE ESTIMATION RESULT IN THE Z AXIS.

	Convergence time (s)	Stabilization time (s)	ARMSEs (N)
GPADKF	3.2980	–	1.1538
EDKF	4.4140	–	3.3211
DKF	Not converge	4.3510	5.6564

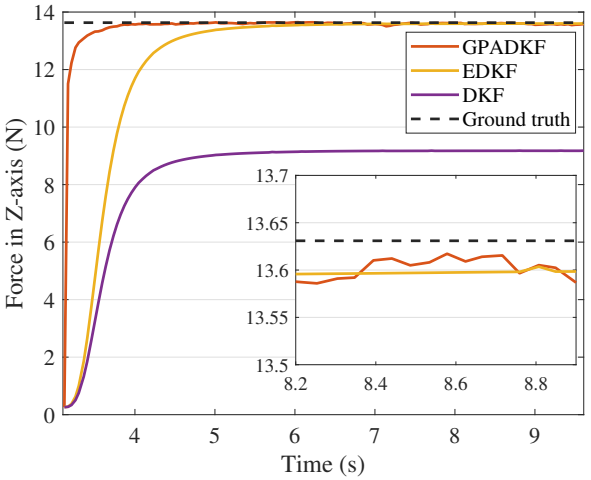

Figure 9. Contact force estimation result in Z-axis under a constant contact scenario.

Fig. 9 illustrates the convergence behavior of the DKF, EDKF, and GPADKF methods. It is observed that both DKF and EDKF exhibit similar initial convergence rates, while the proposed GPADKF demonstrates the highest convergence rate. This can be attributed to the gain auto-tuning mechanism based on the VB approach employed in GPADKF, making it robust to contact force models with inaccurate covariance matrices.

In Table III, we present the convergence time and stabilization time for DKF-based methods with and without residual dynamics compensation, aiming to quantify the transient performance. The convergence time is defined as the moment when the estimate first reaches the 5% error neighborhood of the true value, while the stabilization time is defined as the moment when the estimate first reaches 5% of the steady-state value (which may not necessarily be the true value). The results indicate that the GPADKF outperforms DKF and EDKF, achieving a reduction of 31.9% and 33.8% in convergence (stabilization) time, respectively. Additionally, the GPADKF demonstrates the lowest averaged RMSEs (ARMSEs), further validating its superior performance. A video of the experiments performed can be found at the following link https://youtu.be/0ZPXi4OVcvE.

VII. CONCLUSION

In this paper, the GPADKF method has been proposed for contact force estimation on a robot manipulator, leveraging the benefits of an EGP model with residual dynamics compensation learned using GPs and the VB method for identifying inaccurate noise covariance matrices. Experimental results on the OpenManipulator robot have validated the superiority of GPADKF over the existing force estimation approaches. Our method assumes low-speed motion and small errors in the inertia matrix, allowing for online force estimation without employing acceleration. While our results have supported this assumption, caution should been advised when applying it to different scenarios. A limitation of our approach is that the residual dynamics training have to be performed offline. To address this, future work will explore online model learning through adaptive dynamic programming [55] and advanced distributed filtering techniques [56]–[58] for force estimation in multi-sensor robots. Additionally, we aim to integrate contact force estimation into robot path planning [59] and environmental perception tasks [33], [60].

REFERENCES

[1] L. Santos and R. Cortesao, "Computed-torque control for robotic-assisted tele-echography based on perceived stiffness estimation," *IEEE Trans. Automat. Sci. Eng.*, vol. 15, no. 3, pp. 1337–1354, 2018.
[2] B. Shi, F. Wang, Z. Huo, Y. Tian, R. Cong, and D. Zhang, "Contact force sensing and control for inserting operation during precise assembly using a micromanipulator integrated with force sensors," *IEEE Trans. Automat. Sci. Eng.*, doi: 10.1109/TASE.2022.3195951.
[3] A. Ollero, M. Tognon, A. Suarez, D. Lee, and A. Franchi, "Past, present, and future of aerial robotic manipulators," *IEEE Trans. Robot.*, vol. 38, no. 1, pp. 626–645, 2022.
[4] M. W. Spong, "On the robust control of robot manipulators," *IEEE Trans. Autom. Control*, vol. 37, no. 11, pp. 1782–1786, 1992.
[5] C. Atkeson, H. Chae, and M. John, "Estimation of inertial parameters of manipulator loads and links," *Int. J. Robot. Res.*, vol.5, no. 3, pp. 101–119, 1986.
[6] Y. Han, J. Wu, C. Liu, and Z. Xiong, "An iterative approach for accurate dynamic model identification of industrial robots," *IEEE Trans. Robot.*, vol. 36, no. 5, pp. 1577–1594, 2020.
[7] D. Nguyen-Tuong and J. Peters, "Model learning for robot control: a survey," *Cogn. Process.*, vol. 12, no.4, pp. 319–340, 2011.
[8] A. Carron, E. Arcari, M. Wermelinger, L. Hewing, M. Hutter, and M. N. Zeilinger, "Data-driven model predictive control for trajectory tracking with a robotic arm," *IEEE Robot. Autom. Lett.*, vol. 4, no.4, pp. 3758–3765, 2019.
[9] L. Guo and S. Cao, *Anti-Disturbance Control for Systems with Multiple Disturbances*, New York, USA: CRC Press, 2013.
[10] W. Li, and L. Guo, "Robust particle filtering with time-varying model uncertainty and inaccurate noise covariance matrix," *IEEE Trans. Syst., Man, Cybern., Syst.*, vol. 51, no. 11, pp. 7099–7108, 2021.
[11] L. Guo and S. Cao, "Initial alignment for nonlinear inertial navigation systems with multiple disturbances based on enhanced anti-disturbance filtering," *Int. J. Control*, vol. 85, no. 5, pp. 491–501, 2012.
[12] J. Hu and R. Xiong, "Contact force estimation for robot manipulator using semi-parametric model and disturbance Kalman filter," *IEEE Trans. Ind. Electron.*, vol. 65, no. 4, pp. 3365–3375, 2018.
[13] C. D. Santina, R. L. Truby, and D. Rus, "Data–driven disturbance observers for estimating external forces on soft robots," *IEEE Robot. Autom. Lett.*, vol. 5, no. 4, pp. 5717–5724, 2020.
[14] A. S. Polydoros, L. Nalpantidis, and V. Kruger, "Real-time deep learning of robotic manipulator inverse dynamics," in *IEEE/RSJ International Conference on Intelligent Robots and Systems (IROS)*, Hamburg, Germany, 2015, pp. 3442–3448.
[15] O. Sigaud, C. Salaün, and V. Padois, "On-line regression algorithms for learning mechanical models of robots: A survey," *Rob. Auton. Syst.*, vol. 59, no. 12, pp. 1115–1129, 2011.
[16] S. Vijayakumar, S. Schaal, "Locally weighted projection regression: An o (n) algorithm for incremental real time learning in high dimensional space," in *International Conference on Machine Learning (ICML)*, Morgan Kaufmann, 2000, pp. 288–293.
[17] C. E. Rasmussen and C. K. I. Williams, *Gaussian Processes for Machine Learning*, Cambridge, MA, USA: MIT Press, 2006.
[18] M. P. Deisenroth, R. D. Turner, M. F. Huber, U. D. Hanebeck, and C. E. Rasmussen, "Robust filtering and smoothing with Gaussian processes," *IEEE Trans. Automat. Contr.*, vol. 57, no. 7, pp. 1865–1871, 2012.

IEEE Transactions on Automation Science and Engineering (T-ASE) paper, presented at ICRA 2024, Yokohama, Japan.

[19] J. Ko and D. Fox, "GP-BayesFilters: Bayesian filtering using Gaussian process prediction and observation models," *Auton. Robot.*, vol. 27, no. 1, pp. 75–90, 2008.

[20] L. Hewing, J. Kabzan, and M. N. Zeilinger, "Cautious model predictive control using Gaussian process regression," *IEEE Trans. Control Syst. Technol.*, vol. 28, no. 6, pp. 2736–2743, 2020.

[21] S. Haddadin, A. D. Luca, and A. Albu-Schaffer, "Robot collisions: A survey on detection, isolation, and identification," *IEEE Trans. Robot.*, vol. 33, no. 6, pp. 1292–1312, 2017.

[22] J. Vorndamme, M. Schappler, and S. Haddadin, "Collision detection, isolation and identification for humanoids," in *International Conference on Robotics and Automation (ICRA)*, Singapore, 2017, pp. 4754–4761.

[23] A. Wahrburg, J. Bos, K. D. Listmann, F. Dai, B. Matthias, and H. Ding, "Motor-current-based estimation of Cartesian contact forces and torques for robotic manipulators and its application to force control," *IEEE Trans. Automat. Sci. Eng.*, vol. 15, no. 2, pp. 879–886, 2018.

[24] K. Ohishi, M. Nakao, K. Ohnishi, and K. Miyachi, "Microprocessor controlled dc motor for load-insensitive position servo system," *IEEE Trans. Ind. Electron.*, vol. 34, no. 1, pp. 44–49, 1987.

[25] E. Sariyildiz and K. Ohnishi, "An adaptive reaction force observer design," *IEEE/ASME Trans. Mechatr.*, vol. 20, no. 2, pp. 750–760, 2015.

[26] W. Chen, J. Yang, L. Guo, and S. Li, "Disturbance-observer-based control and related methods—an Overview," *IEEE Trans. Ind. Electron.*, vol. 63, no. 2, pp. 1383–1095, 2016.

[27] W. Chen, "Disturbance observer based control for nonlinear systems," *IEEE/ASME Trans. Mechatron.*, vol. 9, no. 4, pp. 706–710, 2004.

[28] L. Guo and W. Chen, "Disturbance attenuation and rejection for systems with nonlinearity via DOBC approach," *Int. J. Robust Nonlin.*, vol. 15, no. 3, pp. 109–125, 2005.

[29] Y. Zhu, J. Qiao, and L. Guo, "Adaptive sliding mode disturbance observer-based composite control with prescribed performance of space manipulators for target capturing," *IEEE Trans. Ind. Electron.*, vol. 66, no. 3, pp. 1973–1983, 2019.

[30] W. Chen, D. J. Ballance, P. J. Gawthrop, and J. O'Reilly, "A nonlinear disturbance observer for robotic manipulators," *IEEE Trans. Ind. Electron.*, vol. 47, no. 4, pp. 932–938, 2000.

[31] L. Guo, and S. Cao, "Anti-disturbance control theory for systems with multiple disturbances: A survey," *ISA Trans.*, vol. 53, no. 4, pp. 846–849, 2014.

[32] Y. Cui, J. Qiao, Y. Zhu, X. Yu, and L. Guo, "Velocity-tracking control based on refined disturbance observer for gimbal servo system with multiple disturbances," *IEEE Trans. Ind. Electron.*, vol. 69, no. 10, pp. 10311-10321, 2021.

[33] L. Roveda, A. Shahid, N. Lannacci, and D. Piga, "Sensorless optimal interaction control exploiting environment stiffness estimation," *IEEE Trans. Control Syst. Technol.*, vol. 30, no. 1, pp. 218–233, 2021.

[34] L. Roveda, A. Bussolan, F. Braghin, and D. Piga, "6D virtual sensor for wrench estimation in robotized interaction tasks exploiting extended Kalman filter," *Machines*, vol. 8, no. 4, pp. 67–84, 2020.

[35] L. Roveda, D. Riva, G. Bucca, and D. Piga, "Sensorless optimal switching impact/force controller," *IEEE Access*, vol. 9, pp. 158167–158184, 2021.

[36] Y. Wei, W. Li, Y. Yang, X. Yu and L. Guo, "Decoupling observer for contact force estimation of robot manipulators based on enhanced Gaussian process model," in *IEEE International Conference on Cloud Computing and Intelligent Systems (CCIS)*, Chengdu, China, 2022, pp. 1–7.

[37] A. Wahrburg, J. Bos, K. D. Listmann, F. Dai, B. Matthias, and H. Ding, "Motor-current-based estimation of Cartesian contact forces and torques for robotic manipulators and its application to force control," *IEEE Trans. Automat. Sci. Eng.*, vol. 15, no. 2, pp. 879–886, 2018.

[38] B. Siciliano and O. Khatib, *Springer Handbook of Robot*, Amsterdam, Netherlands: Springer, 2016.

[39] V. Sotoudehnejad, A. Takhmar, M. R. Kermani, and I. G. Polushin, "Counteracting modeling errors for sensitive observer-based manipulator collision detection," in *IEEE/RSJ International Conference on Intelligent Robots and Systems (IROS)*, Vilamoura, Portugal, 2012, pp. 4315–4320.

[40] S. Birjandi and S. Haddadin, "Model-adaptive high-speed collision detection for serial-chain robot manipulators," *IEEE Robot. Autom. Lett.*, vol. 5, no. 4, pp. 6544–6551, 2020.

[41] Y. Cui, Y. Yang, Y. Zhu, J. Qiao, and L. Guo, "Composite velocity-tracking control for flexible gimbal system with multi-frequency-band disturbances," *IEEE Trans. Circuits Syst.*, vol. 68, no. 10, pp. 4360–4370, 2021.

[42] R. Hao, J. Wang, J. Zhao, and S. Wang, "Observer-based robust control of 6-DOF parallel electrical manipulator with fast friction estimation," *IEEE Trans. Automat. Sci. Eng.*, vol. 13, no. 3, pp. 1399–1408, 2016.

[43] J. Swevers, W. Verdonck, and J. D. Schutter, "Dynamic model identification for industrial robots," *IEEE Control Syst. Mag.*, vol. 27, no. 5, pp. 58–71, 2007.

[44] S. Wolf and M. Iskandar, "Extending a dynamic friction model with nonlinear viscous and thermal dependency for a motor and harmonic drive gear," in *IEEE International Conference on Robotics and Automation (ICRA)*, Brisbane, 2018, pp. 783–790.

[45] M. Iskandar and S. Wolf, "Dynamic friction model with thermal and load dependency: Modeling, compensation, and external force estimation," in *IEEE International Conference on Robotics and Automation (ICRA)*, Montreal, 2019, pp. 7367–7373.

[46] W. Li, B. Tian, J. Qiao, and L. Guo, "Estimating quasiperiodic disturbance with unknown frequency via expectation-maximization," *IEEE Trans. Cybern.*, vol. 52, no. 7, pp. 6843–6856, 2022.

[47] Y. Huang, Y. Zhang, Z. Wu, N. Li, and J. Chambers, "A novel adaptive Kalman filter with inaccurate process and measurement noise covariance matrices," *IEEE Trans. Automat. Contr.*, vol. 63, no. 2, pp. 594–601, 2018.

[48] A. O'Hagan and J. J. Forster, *Kendall's Advanced Theory of Statistics: Bayesian Inference*, London, U.K.: Arnold, 2004.

[49] F. Qu, X. Zhao, X. Wang, and E. Tian, "Probabilistic-constrained distributed fusion filtering for a class of time-varying systems over sensor networks: A torus-event-triggering mechanism," *Int. J. Syst. Sci.*, vol. 53, no. 6, pp. 1288-1297, 2022.

[50] Z. Hu, J. Hu, H. Tan, J. Huang, and Z. Cao, "Distributed resilient fusion filtering for nonlinear systems with random sensor delay under roundrobin protocol," *Int. J. Syst. Sci.*, vol. 53, no. 13, pp. 2786-2799, 2022.

[51] G. Abdelnour, S. Chand, and S. Chiu, "Applying fuzzy logic to the Kalman filter divergence problem," in *IEEE Systems Man and Cybernetics Conference (SMC)*, Le Touquet, 1993, pp. 630–635.

[52] Q. Zhang and Y. Zhou, "Recent advances in non-Gaussian stochastic systems control theory and its applications," *Int. J. Network Dyn. Intell.*, vol. 1, no. 1, pp. 111-119, 2022.

[53] T. D. Bui, J. Yan, and R. E. Turner, "A unifying framework for Gaussian process pseudo-point approximations using power expectation propagation," *J. Mach. Learn. Res.*, vol. 18, no. 1, pp. 3649–3720, 2017.

[54] X. Li, S. Feng, N. Hou, R. Wang, H. Li, M. Gao, and S. Li, "Surface microseismic data denoising based on sparse autoencoder and Kalman filter," *Syst. Sci. & Control. Eng.*, vol. 10, no. 1, pp. 616-628, 2022.

[55] X. Wang, Y. Sun, and D. Ding, "Adaptive dynamic programming for networked control systems under communication constraints: a survey of trends and techniques," *Int. J. Network Dyn. Intell.*, vol. 1, no. 1, pp. 85-98, 2022.

[56] X. Meng, Y. Chen, L. Ma and H. Liu, "Protocol-based variance-constrained distributed secure filtering with measurement censoring," *Int. J. Syst. Sci.*, vol. 53, no. 15, pp. 3322-3338, 2022.

[57] P. Wen, X. Li, N. Hou and S. Mu, "Distributed recursive fault estimation with binary encoding schemes over sensor networks," *Syst. Sci. & Control. Eng.*, vol. 10, no. 1, pp. 417-427, 2022.

[58] M. Li, J. Liang, and F. Wang, "Robust set-membership filtering for two-dimensional systems with sensor saturation under the Round-Robin protocol," *Int. J. Syst. Sci.*, vol. 53, no. 13, pp. 2773-2785, 2022.

[59] L. Xu, B. Song and M. Cao, "A new approach to optimal smooth path planning of mobile robots with continuous-curvature constraint," *Comput. Sci. Inf. Syst.*, vol. 9, no. 1, pp. 138–149, 2021.

[60] L. Roveda, and P. Dario, "Sensorless environment stiffness and interaction force estimation for impedance control tuning in robotized interaction tasks," *Auton. Robot.*, vol. 45 no.3, pp. 371–388, 2021.

IEEE Transactions on Automation Science and Engineering (T-ASE) paper, presented at ICRA 2024, Yokohama, Japan.

Yanran Wei received the B.Eng. degree from Dalian University of Technology, China in 2018. She is currently working toward the Ph.D. degree in control theory and control engineering from the School of Automation Science and Electrical Engineering, Beihang University, China. Her research interests include anti-disturbance control and filtering, Bayesian estimation, force estimation, and robot learning.

Shangke Lyu received the B.Eng. degree from Sichuan University, Sichuan, China in 2014 and the Ph.D. degree in robotics and automation from Nanyang Technological University, Singapore, in 2019. From 2019 to 2022, he was a postdoctoral fellow with Hangzhou Innovation Institute of Beihang University. Currently, he is a Research Assistant Professor with Westlake University. His research interests include robot motion control, human-robot interaction, adaptive control, learning control and reinforcement learning.

Wenshuo Li received the B.E. degree in automation from Shandong University, China and the Ph.D degree in control theory and control engineering from Beihang University, China, in 2012 and 2020 respectively. He is currently a Postdoctoral Research Fellow with Hangzhou Innovation Institute, Beihang University, Hangzhou, China. From Jan. 2016 to Jan. 2017, he was an international researcher in the Department of Computer Science, Brunel University London, UK. His research interests include nonlinear filtering, anti-disturbance control and filtering, networked control systems, and Bayesian estimation. He is an active reviewer for many international journals.

Xiang Yu received the B.S., M.S., and Ph.D. degrees in automation science and engineering from Northwestern Polytechnical University, Xian, China, in 2003, 2004, and 2008, respectively. He is currently a Professor with the School of Automation Science and Electrical Engineering, Beihang University, Beijing, China. He was a Post-Doctoral Research Fellow with the Department of Electrical and Computer Engineering, Western University, London, ON, Canada, and a Research Associate with the Department of Mechanical, Industrial and Aerospace Engineering, Concordia University, Montreal, QC, Canada. He has authored over 40 prestigious journal papers and a monograph, including IEEE Transactions, AIAA Journals, and Progress in Aerospace Sciences. His current research interests include safety control of aerospace engineering systems, autonomous navigation and control of unmanned aerial vehicles. Prof. Yu was a recipient of the Recruitment Program for Young Professionals, the Best Paper and Best Paper Finalist at international conferences. He has also served as the Associate Editor of Asian Journal of Control, Associate Editor of Chinese Journal of Aeronautics, Program Co-Chair, Invitation Chair, and IPC Member of several academic conferences.

Lei Guo (Fellow, IEEE) was born in Qufu, China, in 1966. He received the B.S. and M.S. degrees from Qufu Normal University, Qufu, in 1988 and 1991, respectively, and the Ph.D. degree in control engineering from Southeast University, Nanjing, China, in 1997. From 1991 to 1994, he was a Lecturer with Qingdao University, Qingdao, China. From 1997 to 1999, he was a Postdoctoral Fellow with Southeast University. From 1999 to 2000, he was a Research Fellow with IRCCyN, Nantes, Frances. From 2000 to 2003, he was a Research Fellow with the University of Glasgow, Glasgow, U.K., Loughborough University, Loughborough, U.K., and the University of Manchester Institute of Science and Technology, Manchester, U.K. In 2004, he joined the Institute of Automation, Southeast University, as a Professor. In 2006, he became a Professor with the School of Instrumentation and Opto-Electronics Engineering, Beihang University, Beijing, China, where he is currently with the School of Automation Science and Electronic Engineering. He is an Awarder of the National Science Fund for Distinguished Young Scholars of China and a Changjiang Distinguished Professor of the Ministry of Education of China. He has published more than 120 papers and one monograph and served as an Editor for five journals. His research interests include robust control, stochastic systems, fault detection, filter design, and nonlinear control with their applications to aerospace systems.